Cholangiocarcinoma and Malignant Biliary Obstruction

81

Tae Kyoung Kim, Hyun-Jung Jang, Martin O'Malley, and Korosh Khalili

Introduction

Cholangiocarcinomas (CC) are malignant neoplasms arising from biliary epithelium. Although it is an uncommon malignancy, it is the second most common primary hepatobiliary malignancy and the incidence is increasing globally (Malhi and Gores 2006). CC can be classified according to anatomic location as intrahepatic or extrahepatic, with extrahepatic further classified as hilar and distal extrahepatic. Familiarity with the diverse imaging and clinical manifestations depending on different morphologic types of CC is important for accurate diagnosis and assessment of resectability. The morphologic classification proposed by the Liver Cancer Study Group of Japan (Yamasaki 2003) classifies intrahepatic CC as mass-forming, periductal-infiltrating, and intraductal-growing types.

Risk factors for CC include primary sclerosing cholangitis (PSC), chronic hepatolithiasis, recurrent pyogenic cholangitis (RPC), choledocholithiasis, parasitic biliary infestation, viral hepatitis, bile duct adenoma, biliary papillomatosis, Caroli's disease, choledochal cyst, Thorotrast, smoking, and chronic typhoid carrier state. However, in many cases, no risk factor is identified. PSC is a common risk factor for the development of CC in Western countries (Burak et al. 2004), whereas parasitic infestation by *Clonorchis sinensis* and *Opisthorchis viverrini* (Kim et al. 2006, 2007) and RPC (Kim et al. 2006) are important risk factors in the East and Southeast Asia. Chronic hepatitis B and C virus infections have recently been recognized as risk factors for intrahepatic CC in both the East and West (Malhi and Gores 2006).

Radiological imaging plays a crucial role in the diagnosis and staging of CC and malignant biliary obstruction. Ultrasound is often used as the initial imaging test for suspected biliary obstruction. CT is most commonly used for the diagnosis and staging of the disease as well as follow-up. MR imaging is often helpful as an adjuvant imaging modality as it can provide superior tissue characterization and high-quality noninvasive cholangiography. In practice, a multimodality approach is helpful for challenging cases.

This chapter reviews typical imaging patterns of CC and other causes of malignant biliary obstruction on cross-sectional imaging.

Mass-Forming Intrahepatic Cholangiocarcinoma

Pathology and Clinical Features

Mass-forming type is the most common morphologic type of intrahepatic CC. The tumor easily invades and penetrates the bile duct wall and grows outward to form a nodular mass in the liver parenchyma. The mass contains abundant desmoplastic reaction and fibrosis particularly in the center. Viable tumor cells are usually located at the periphery of the tumor. Mass-forming intrahepatic CC typically presents with a palpable mass or nonspecific symptoms such as fever, night sweats, and weight loss, or right upper

T.K. Kim (✉) • H.-J. Jang • M. O'Malley • K. Khalili
Department of Medical Imaging, Toronto General Hospital, University of Toronto, Toronto, ON, Canada

B. Hamm, P. R. Ros (eds.), *Abdominal Imaging*, DOI 10.1007/978-3-642-13327-5_146,
© Springer-Verlag Berlin Heidelberg 2013

quadrant abdominal pain. Obstructive jaundice occurs when the tumor involves the hepatic hilum.

Image Findings

Ultrasound

Ultrasound is frequently performed for initial evaluation of abdominal symptoms. Mass-forming intrahepatic CC is seen as a large, homogeneous solid mass with variable echogenicity. Surveillance ultrasound for hepatocellular carcinoma (HCC) occasionally detects small intrahepatic CC without clinical symptoms as hepatitis B or C is now recognized as a risk factor for CC (Kim et al. 2007). Contrast-enhanced ultrasound (CEUS) using microbubble contrast agents usually shows diffuse or peripheral hypervascularity of the mass followed by rapid washout (Fig. 81.1) beginning from less than 75 s after contrast injection. Washout timing of CC is faster than HCC which typically shows later washout (Bhayana et al. 2010). The mass shows marked hypoechogenicity in the late phase (>3 min) of CEUS which is distinctly different from contrast-enhanced CT or MR imaging that shows persistent positive enhancement in the delayed phase (>3–5 min) due to accumulation of the contrast agent in the interstitial space (Fig. 81.1). Lack of delayed enhancement in CEUS is due to the strictly intravascular nature of microbubble contrast agent (Wilson et al. 2007).

CT

Mass-forming CC usually shows marked hypoattenuation in the arterial phase and portal venous phase with or without thin rim-like enhancement (Fig. 81.2) (Kim et al. 1997). However, the mass infrequently shows arterial hypervascularity potentially mimicking the appearance of HCC (Fig. 81.1) (Kim et al. 1997, 2007). The central portion of the tumor shows substantial enhancement in the delayed phase (>3–5 min) due to abundant fibrous stroma (Asayama et al. 2006). Small intrahepatic metastases are frequently seen (Fig. 81.2). Capsular retraction due to prominent desmoplastic reaction is occasionally seen and is one of the differentiating features from HCC (Fig. 81.3). Intrahepatic bile ducts peripheral to the tumor can be dilated due to obstruction. Associated parasitic infestation in endemic areas can be seen as diffuse mild dilatation of the intrahepatic bile ducts without obstructing lesions (Choi et al. 1998, 2006). Diffuse, severe dilatation of the entire intrahepatic bile ducts is seen when the tumor invades the hepatic hilum, obstructing the bile duct confluence (Fig. 81.4). Narrowing or obstruction of the portal or hepatic vein due to tumor invasion or extrinsic compression is frequently seen when the tumor is centrally located. Metastasis to the abdominal lymph nodes and peritoneum is common (Fig. 81.4). CT scan tends to underestimate nodal involvement (Vilgrain 2008).

MR Imaging

Mass-forming intrahepatic CC is mildly hyperintense on T2-weighted images and hypointense on T1-weighted images. Peripheral rim-like enhancement is frequently seen in the arterial phase of contrast-enhanced T1-weighted images, and gradual and persistent central enhancement is seen over time similar to CT (Fig. 81.3). MR imaging is often used for surveillance of the development of CC in patients with PSC. Diagnosis of CC in PSC is challenging due to preexisting biliary strictures and thickening. CC in PSC is most commonly seen as a parenchymal mass or dominant and progressive biliary stricture with dilatation (Fig. 81.5) (Seo et al. 2009). CC in RPC most commonly manifests as a mass-forming intrahepatic CC frequently in atrophic liver segments and less commonly as focally thickened bile duct with enhancement (Fig. 81.6) (Kim et al. 2006). MR imaging is helpful to differentiate mass-forming CC from abscess in patients with RPC as a liver abscess typically shows central cystic change with bright hyperintensity and a thick wall on T2-weighted images. However, immature or healing abscess may simulate the appearance of CC (Khalili et al. 2003).

Hilar and Distal Extrahepatic Cholangiocarcinoma

Pathology and Clinical Features

Periductal-infiltrating type is the most common in hilar CC. The tumor grows along the bile duct wall, resulting in concentric thickening of the bile duct wall without forming a nodular mass (Lim 2003). The involved bile ducts are narrowed or obstructed and the upstream bile ducts are dilated. Distal extrahepatic CC most commonly manifests as a small nodular

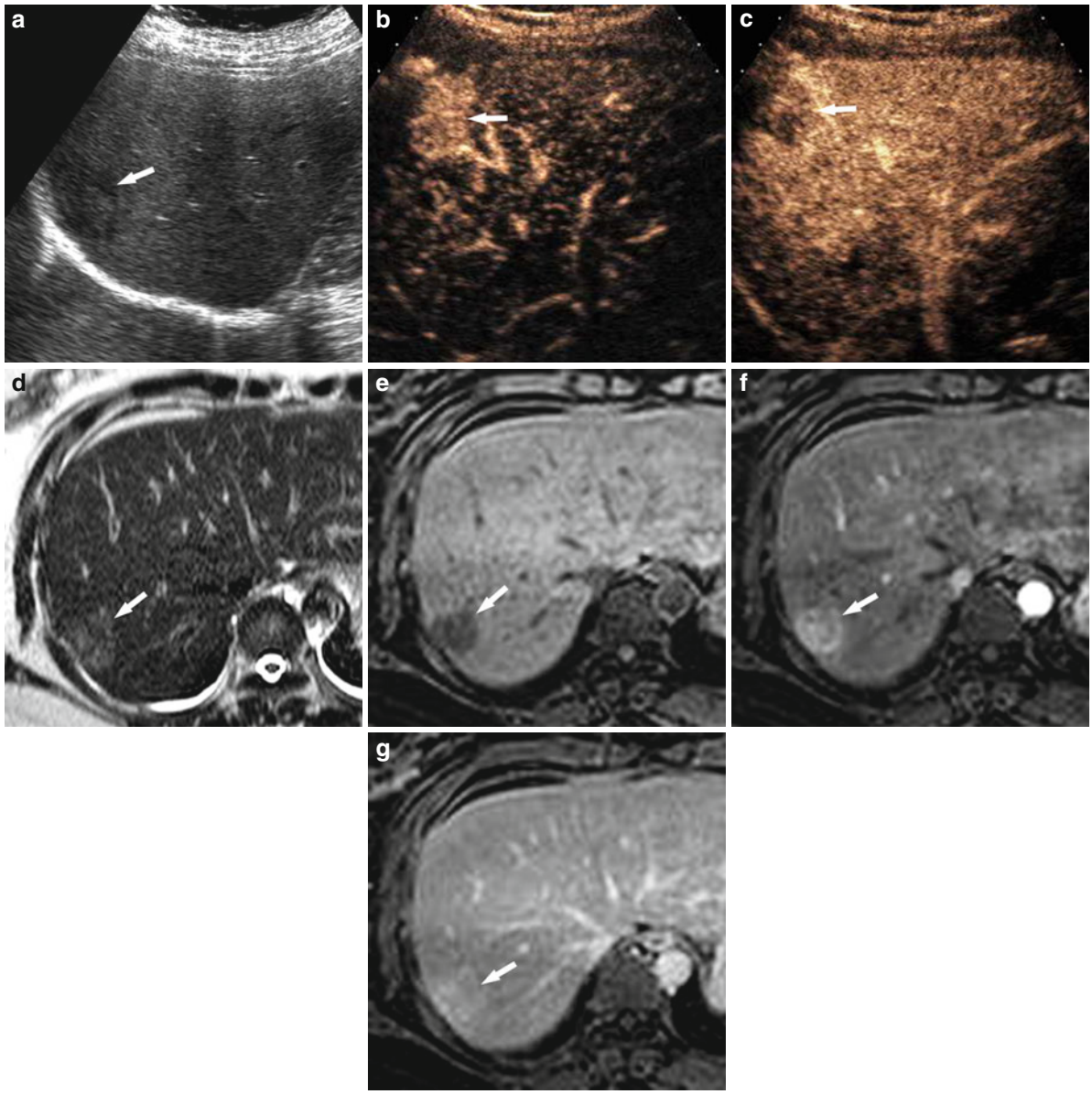

Fig. 81.1 Small hypervascular intrahepatic mass-forming cholangiocarcinoma. (**a**) Transverse ultrasound scan shows a hypoechoic mass (*arrow*). (**b–c**) Arterial-phase contrast-enhanced ultrasound scan (**b**) shows diffuse hypervascularity of the mass (*arrow*) followed by rapid washout at 23 s after injection of contrast (**c**). (**d–e**) The mass (*arrow*) is mildly hyperintense on T2-weighted MR image (**d**) and hypointense on T1-weighted image (**e**). (**f–g**) The mass (*arrow*) is hypervascular relative to the liver in the arterial phase (**f**) and shows sustained positive enhancement at 5 min after injection of contrast (**g**)

mass-forming CC, although other morphologic types are occasionally seen (Seo et al. 2009). Patients with extrahepatic CC mostly present with jaundice. The tumors are usually small because they are discovered early due to obstructive jaundice. Surgical resection with histologically negative resection margin offers the best chance of long-term survival. Resection of hilar CC includes a partial hepatectomy of the predominantly involved lobe of the liver. Pancreaticoduodenectomy is performed for distal extrahepatic CC involving the intrapancreatic portion of the CBD. Therefore, imaging interpretation of extrahepatic CC

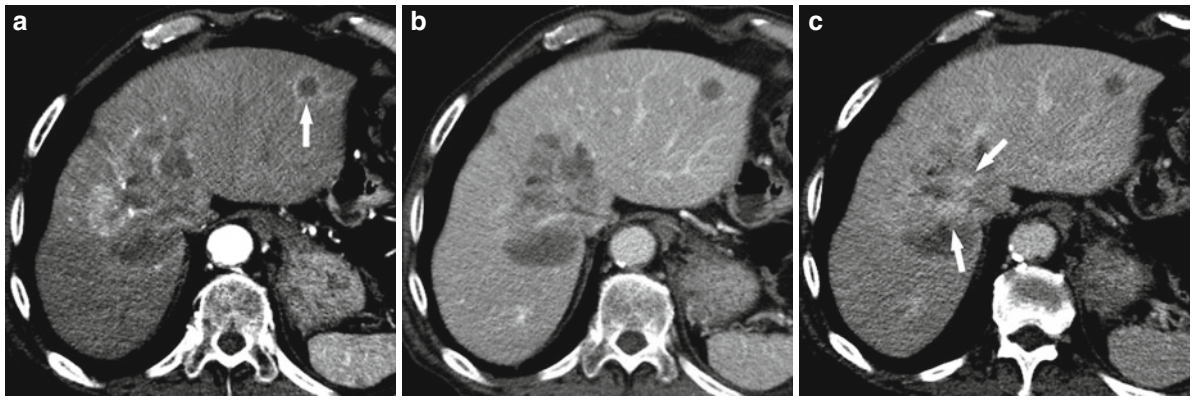

Fig. 81.2 Large mass-forming intrahepatic cholangiocarcinoma. (**a**–**c**) CT scans in the arterial (**a**), portal venous (**b**), and delayed (**c**) phases show a large heterogeneous mass in the dome of the right lobe and a small metastatic nodule (*arrow* in (**a**)) in the left lobe. The large mass shows minimal peripheral enhancement in the arterial phase and substantial enhancement in the central portion of the mass in the delayed phase (*arrows* in (**c**))

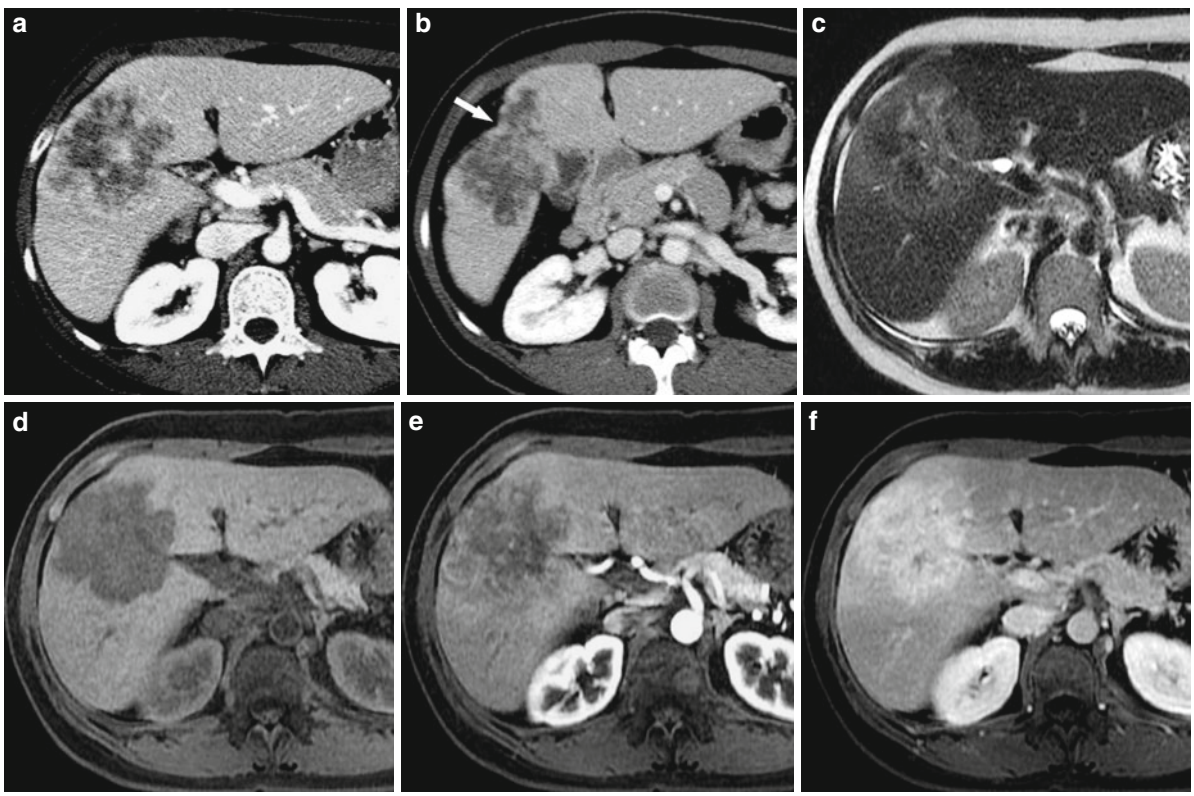

Fig. 81.3 Large mass-forming intrahepatic cholangiocarcinoma. (**a**) CT scan in the portal venous phase shows a large heterogeneous hypoattenuating mass in the liver. (**b**) Capsular retraction (*arrow*) is seen along the surface of the mass at a lower level. (**c**) T2-weighted MR image shows a mildly hyperintense mass with central hypointense area due to dense fibrosis. (**d**) The mass is hypointense on T1-weighted image. (**e**) There is subtle peripheral enhancement of the mass on the arterial-phase contrast-enhanced T1-weighted MR image. (**f**) The entire mass shows hyperenhancement relative to the liver in the delayed phase (5 min after injection of contrast)

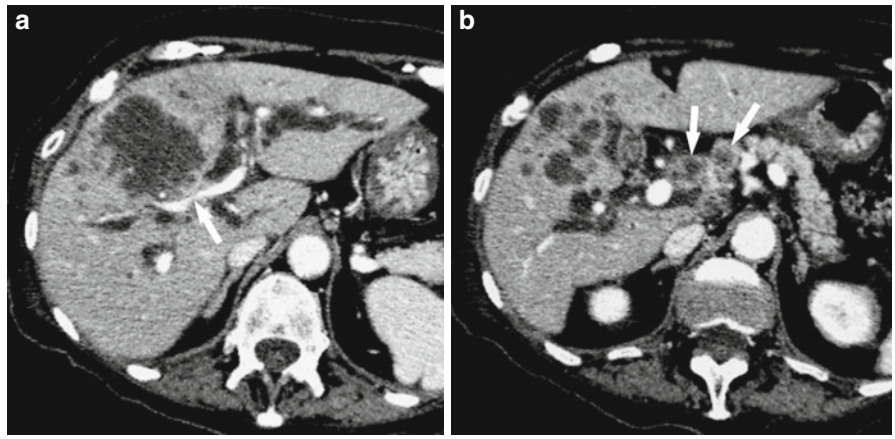

Fig. 81.4 Large mass-forming intrahepatic cholangiocarcinoma with hilar invasion. (**a**) CT scan in the portal venous phase shows a large markedly hypoattenuating mass which invades the hepatic hilum and obstructs hilar bile duct confluence (*arrow*). (**b**) There are multiple rim-enhancing enlarged lymph nodes (*arrows*) in the hepatoduodenal ligament, in keeping with metastases

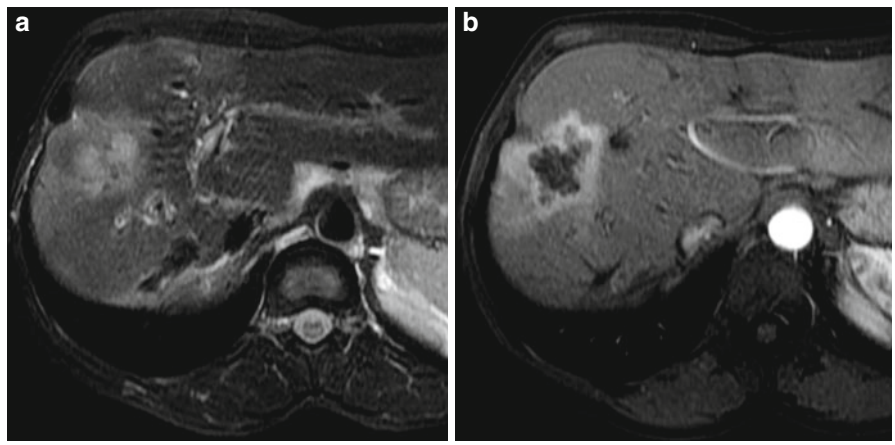

Fig. 81.5 Mass-forming intrahepatic cholangiocarcinoma in primary sclerosing cholangitis. (**a**) T2-weighted MR image shows a heterogeneous mildly hyperintense mass in the right lobe of the liver. The right lobe of the liver is atrophic secondary to long-standing primary sclerosing cholangitis. (**b**) Contrast-enhanced T1-weighted image in the arterial phase shows a rim-like enhancement of the mass

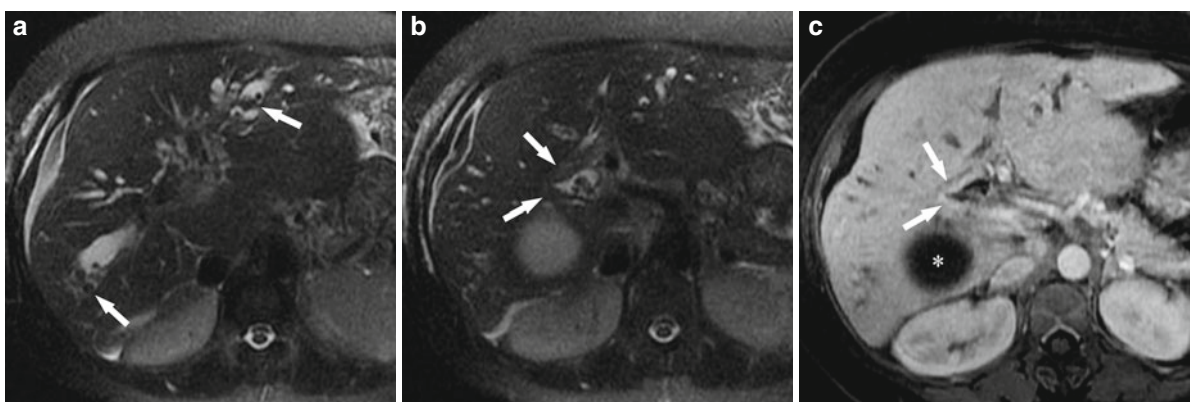

Fig. 81.6 Cholangiocarcinoma in recurrent pyogenic cholangitis. (**a**) T2-weighted MR image shows dilated intrahepatic bile ducts that contain multiple calculi (*arrows*). (**b**) T2-weighted MR image at a lower level shows focal thickening (*arrow*) of the right hepatic duct that contains calculi. (**c**) Contrast-enhanced T1-weighted image in the portal venous phase shows substantial enhancement of the thickened right hepatic duct (*arrow*), representing cholangiocarcinoma. Note an abscess (*) in the right lobe

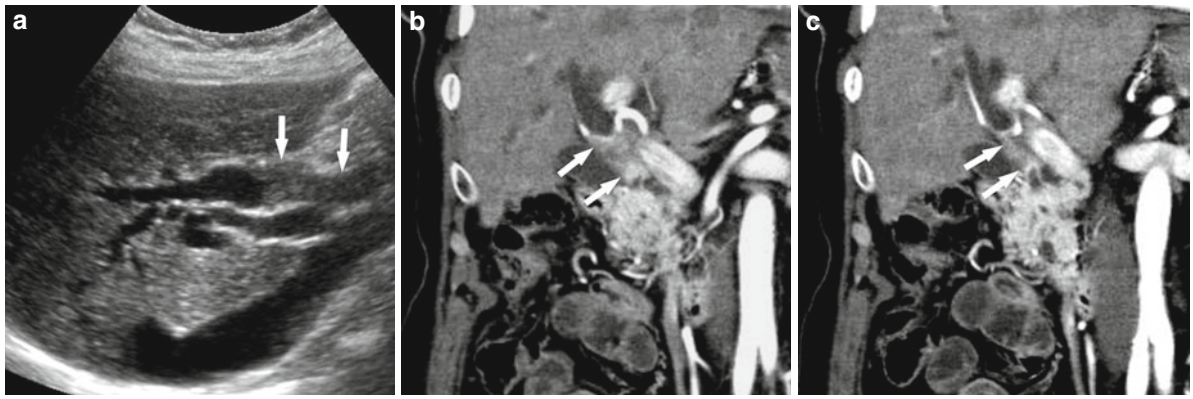

Fig. 81.7 Extrahepatic cholangiocarcinoma involving common bile duct. (**a**) Oblique ultrasound scan shows a hypoechoic mass (*arrows*) involving the mid common bile duct with upstream bile duct dilatation. (**b–c**) Two coronal CT scans clearly demonstrates the extent of the mass (*arrows*) which extends from a few centimeter below hilar bile duct confluence to about 1 cm above the beginning of the intrapancreatic portion of common bile duct

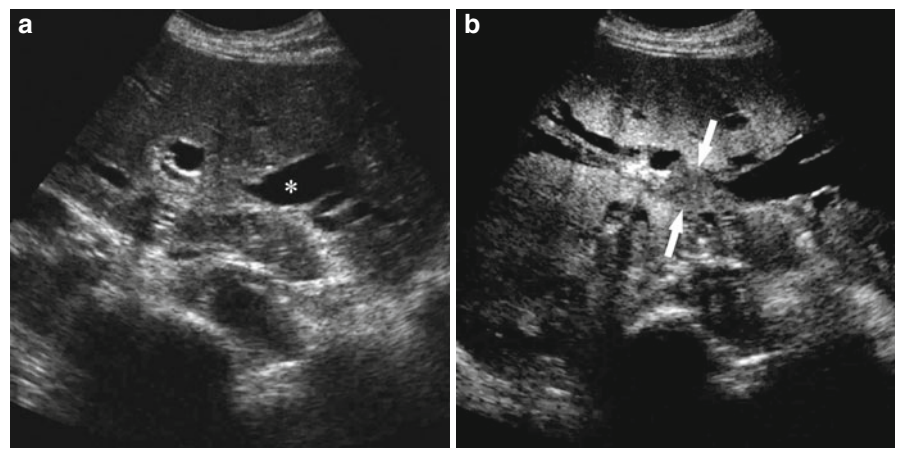

Fig. 81.8 Hilar periductal-infiltrating cholangiocarcinoma. (**a**) Transverse ultrasound scan shows separation of the right and left hepatic ducts and dilatation of the left hepatic duct (*) without definite identifiable mass. (**b**) Contrast-enhanced ultrasound in the late phase demonstrates an infiltrative mass (*arrows*) at the hilar bile duct confluence which is hypoechoic relative to the normal liver

should focus on tumor resectability by detailed evaluation of the tumor extent in the bile duct, local vascular invasion, and distant metastasis.

Image Findings

Ultrasound

Ultrasound is usually performed for initial evaluation in patients with jaundice. Ultrasound is reliable in detecting biliary obstruction and to determine the level of obstruction (Fig. 81.7). Hilar CC is often isoechoic to the liver, making it difficult to visualize the tumor itself. Real-time imaging with slow sweeping through the hepatic hilum can demonstrate separation and dilatation of the right and left hepatic ducts as well as a thickened bile duct or abnormal soft tissue lesion at the area of obstruction. CEUS can help to detect and localize the tumor as the tumor stands out as a perfusion defect in the portal venous phase when the liver shows homogeneous enhancement (Fig. 81.8) (Khalili et al. 2003). Meticulous scanning technique is required to visualize distal extrahepatic CC as it is often obscured by bowel. CT or MR imaging is performed for further characterization of biliary obstruction and staging when extrahepatic CC is suspected on ultrasound.

CT

Thin-section contrast-enhanced CT, ideally with a multislice CT (MSCT) scanner, is important for the diagnosis and staging of extrahepatic CC. MSCT is excellent for localizing hilar CC by demonstrating focal thickening or a mass with substantial

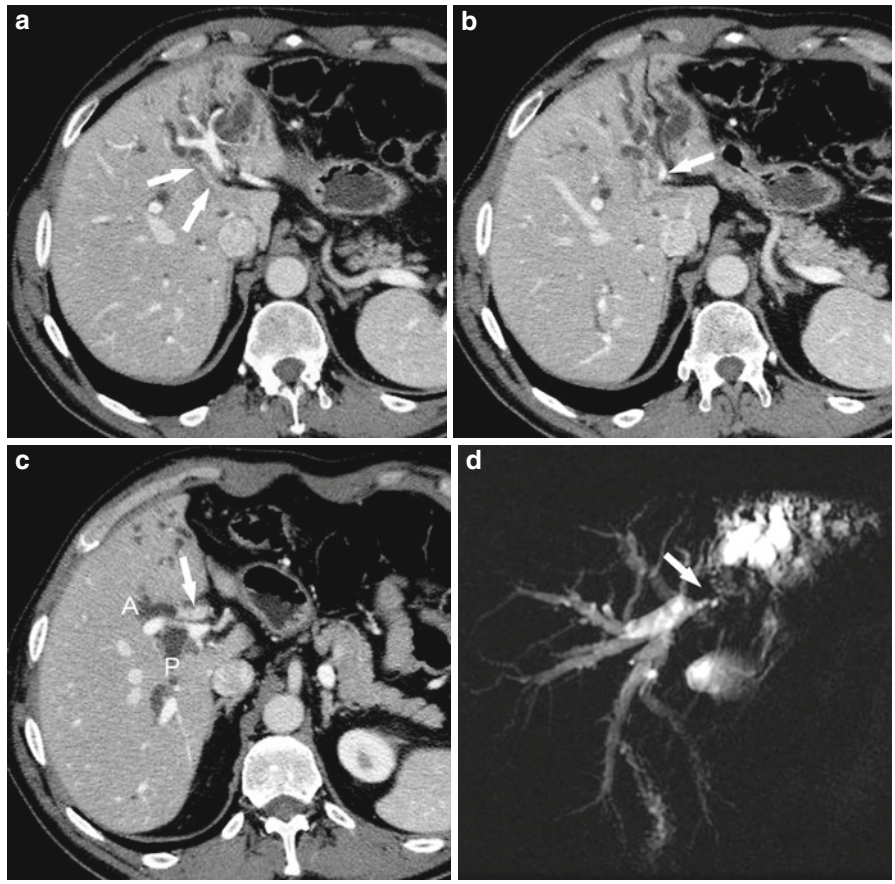

Fig. 81.9 Hilar periductal-infiltrating cholangiocarcinoma. (**a**) CT scan in the portal venous phase shows an ill-defined perihilar mass (*arrows*) replacing the area of the left hepatic duct, which involves the secondary bile duct confluence in the left lobe resulting in severe biliary dilatation and atrophy of the left lobe. (**b**) The perihilar mass is encasing and narrowing the proximal portion of the left portal vein (*arrow*), indicating left portal vein invasion. (**c**) The infiltrative mass (*arrow*) is also involving the secondary bile duct confluence in the right lobe separating anterior (*A*) and posterior (*P*) segmental branch of intrahepatic bile duct. (**d**) Oblique coronal thick-slab single-shot T2-weighted MRC provides a comprehensive view of hilar bile duct obstruction (*arrow*) and intrahepatic biliary dilatation

enhancement accompanied by upstream biliary dilatation (Fig. 81.9) (Han et al. 2002). MSCT is useful to determine the tumor extent and assess the relationship between the tumor and hepatic hilar structures. This is usually best evaluated on PVP images facilitated by multiplanar reformat (MPR) images (Uchida et al. 2005; Chen et al. 2006). A detailed evaluation of axial and coronal thin-section CT images enables assessment of tumor involvement of the primary and secondary bile duct confluence (Fig. 81.9). The longitudinal tumor extent of a distal extrahepatic CC is critical to determine the surgical planning and is best evaluated by coronal or oblique coronal MPR images (Fig. 81.7) (Seo et al. 2009). However, it is recognized that the overall accuracy of CT is limited mainly due to underestimation of longitudinal tumor extent when compared with the pathological results (Seo et al. 2009; Lee et al. 2006). Vascular invasion is diagnosed when there is vessel occlusion, stenosis or contour deformity associated with tumor contact, or greater than 50% perimeter contact with the tumor (Fig. 81.9) (Lee et al. 2006). Bilateral tumor invasion to secondary bile duct confluence or major hilar vessels was previously considered unresectable; however, a curative resection is now often attempted depending on the remaining liver volume, the length of vascular invasion, and anatomic configuration of the bile ducts with reasonable outcomes (Lee et al. 2006).

MR

MR cholangiography (MRC) is an excellent technique to visualize biliary obstruction. T2-weighted thick-slab single-shot MRC with multiple rotational views in any desired scanning plane is the most commonly used technique, providing consistent and comprehensive visualization of the bile duct morphology (Fig. 81.9). T2-weighted respiratory-triggered three-dimensional MRC is also useful (Fig. 81.10) but is more prone to failure due to motion artifact. MRC shows good agreement (87.9%) with percutaneous transhepatic cholangioscopy to determine the extent of biliary involvement of hilar CC (Lee et al. 2002) but has

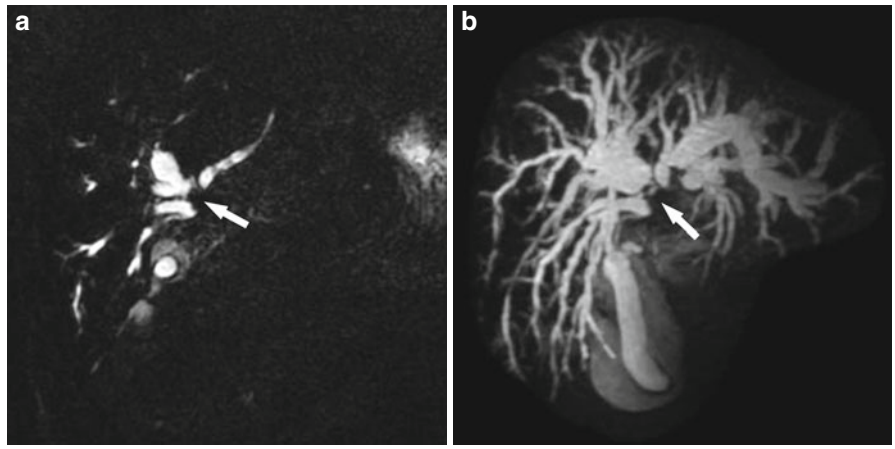

Fig. 81.10 Hilar periductal-infiltrating cholangiocarcinoma. (**a**) Coronal source image of three-dimensional T2-weighted respiratory-triggered MRC shows dilated intrahepatic bile ducts by an obstruction (*arrow*) at the hilum. (**b**) Oblique coronal maximum intensity projection image produced by multiple source images demonstrates hilar bile duct obstruction (*arrow*) and severe dilatation of intrahepatic bile ducts

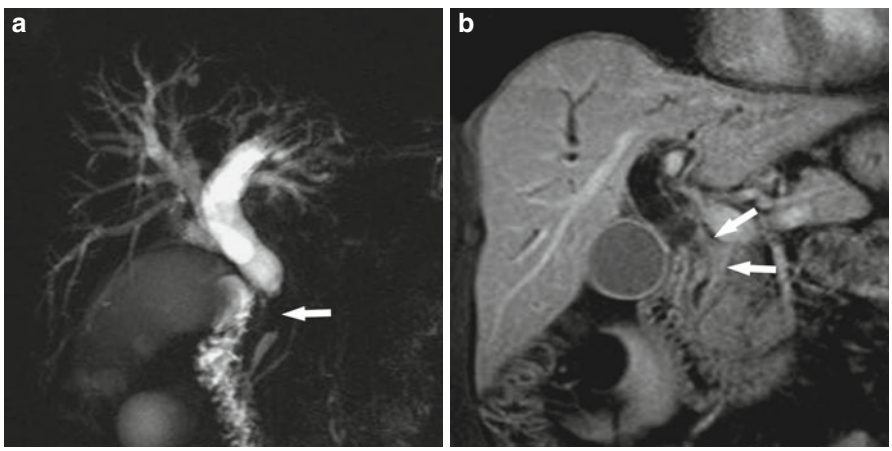

Fig. 81.11 Cholangiocarcinoma in the distal common bile duct. (**a**) Coronal thick-slab single-shot T2-weighted MRC shows an abrupt, lengthy stricture (*arrow*) in the distal common bile duct with upstream biliary dilatation. (**b**) Coronal contrast-enhanced T1-weighted image shows marked thickening and enhancement of the involved segment of the CBD (*arrows*)

a limited diagnostic accuracy (71.4%) when compared with surgical and pathological results particularly due to underestimation of the tumor extent (Cho et al. 2007).

Combined use of MRC and multiphase contrast-enhanced T1-weighted imaging can provide a reliable preoperative evaluation of hilar CC. The evaluation of both MRC and contrast-enhanced T1-weighted images can improve staging accuracy of hilar CC (Masselli et al. 2008). MRC becomes unreliable when a biliary drainage catheter is present, resulting in decompressed bile ducts, pneumobilia, and thickened bile ducts secondary to periductal inflammation, that may mimic or obscure tumor.

MRC may be helpful to differentiate between benign and malignant strictures in the distal extrahepatic bile duct: a lengthy stricture with irregular margin and asymmetric narrowing suggests CC (Fig. 81.11), and a short segment with symmetric narrowing suggests benign cause (Park et al. 2004). However, one should be aware that overlap in the appearances of benign and malignant biliary strictures does exist.

Intraductal-Growing Cholangiocarcinoma

Pathology and Clinical Features

Intraductal-growing CC is the least common morphologic type of CC and occurs in both intrahepatic and extrahepatic bile ducts. The tumors are usually small papillary or polypoid lesions, often spreading superficially along the mucosal surface. The tumors are often

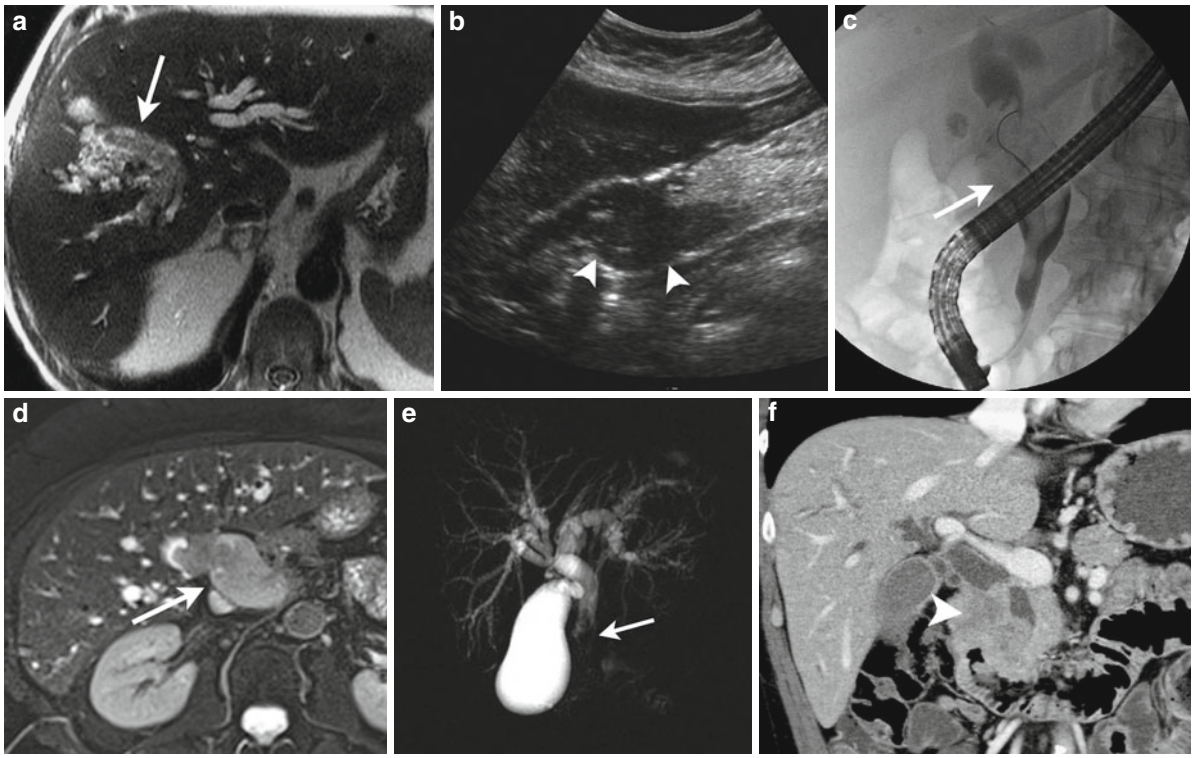

Fig. 81.12 Spectrum of intraductal-growing cholangiocarcinoma. Intrahepatic (**a**) axial T2-weighted MR image depicts a branching papillary mass (*arrow*) growing within the right intrahepatic bile ducts. *Mid CBD* (**b**–**d**) sagittal ultrasound, ERCP, and axial T2-weighted MRI image show a large polypoid mass within, obstructing and expanding the duct (*arrows*). Distal CBD (**e**) thick-slab MRC image demonstrates a polypoid tumor (*arrow*) differentiated from stones by enhancement (not shown). Invasive papillary cholangiocarcinoma (**f**) coronal enhanced CT image showing a large mass extending from the CBD into the duodenum (*arrowhead*)

confined within the bile duct without invasion to the adjacent liver parenchyma. The majority of papillary intraductal tumors do not produce enough mucin to be detected by clinical symptoms, imaging, or gross examination. However, a large amount of mucin is occasionally produced and excreted into the bile duct lumen, resulting in partial biliary obstruction due to thick mucin (Lim 2003). The classification and clinical significance of papillary tumors without and with gross mucin production is currently under intense study but has not been finalized (Ohtsuka et al. 2011).

Morphologically, the appearance of the tumor depends on the location (intrahepatic vs. extrahepatic ducts), extent (focal vs. multifocal mucosal disease), and production of gross mucin (Kim et al. 2011). Tumors without gross production of mucin (most common type) will appear as an intraductal mass causing upstream dilatation (Fig. 81.12). Occasionally, the tumor will obstruct and fill a peripheral hepatic duct with mild obstruction (Fig. 81.13). Mucin-producing tumors affecting the peripheral ducts can cause aneurysmal dilatation of the duct with polypoid mass protruding into it (Fig. 81.14), which can be easily misdiagnosed as a cystic tumor. Communication with the biliary tree, tubular appearance, and mild dilatation of the distal bile duct can help to lead to a correct diagnosis. Rarely, mucin-producing tumor affecting the central bile ducts is seen causing diffuse and marked biliary dilatation with or without a grossly visible papillary mass (Fig. 81.14); the biliary mucosa is often diffusely affected.

Image Findings

Ultrasound

The combination of high spatial and contrast resolution makes ultrasound particularly well suited to

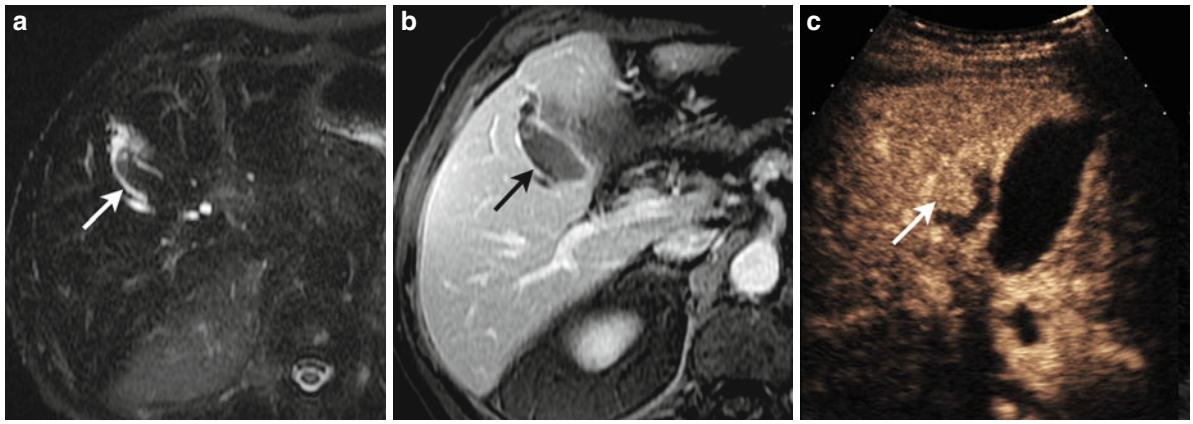

Fig. 81.13 Intraductal-growing cholangiocarcinoma in a peripheral duct (**a**) Axial heavily T2-weighted MRC image showing a distended duct filled with a polypoid mass (*arrow*). (**b**) Corresponding axial T1-weighted image with intravenous contrast shows little enhancement in the mass (*arrow*), making differentiation from debris difficult. (**c**) Contrast-enhanced ultrasound with excellent contrast resolution allows easy detection of the enhancing tumor (*arrow*), adjacent to the gallbladder

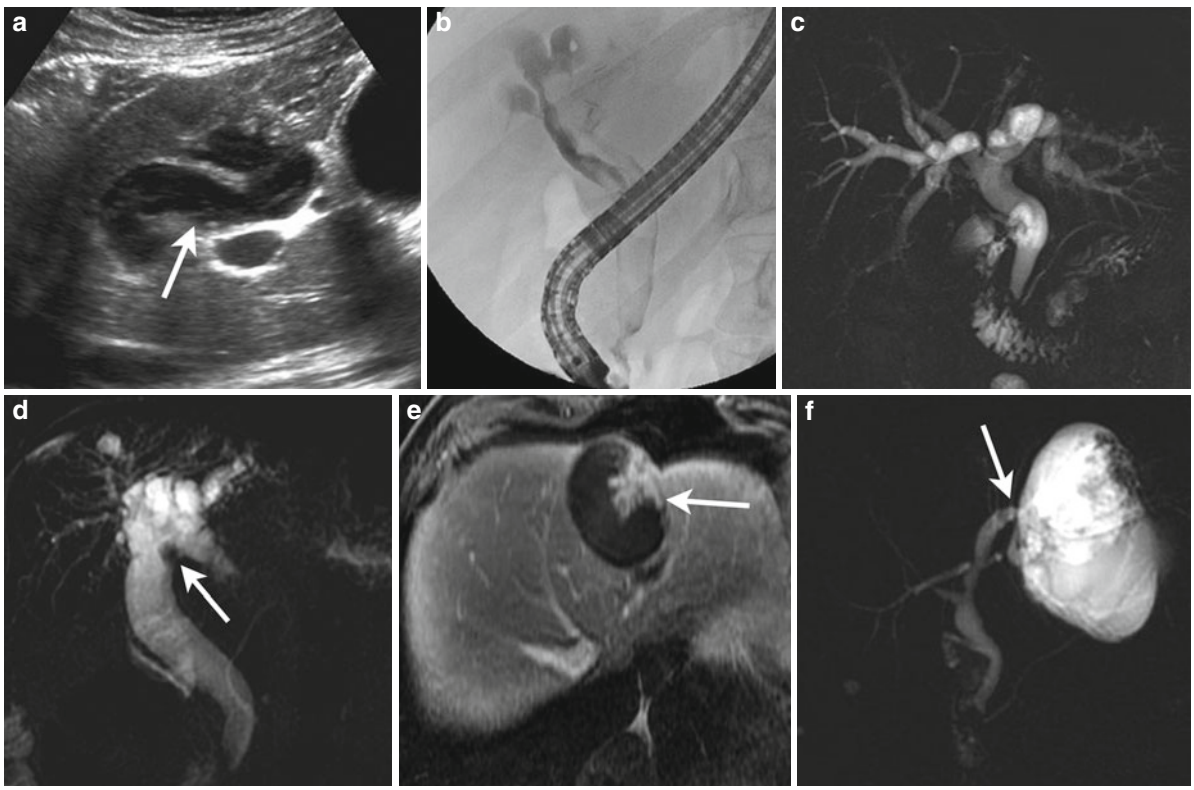

Fig. 81.14 Spectrum of cholangiocarcinoma with excess mucin production. Diffuse disease with no visible mass (**a**) Longitudinal ultrasound image of the CBD shows a distended duct with layering contents, typical for mucin. (**b**) ERCP image shows the mass-like filling defect within the bile duct, representing mucin. (**c**) Thick-slab MRC image depicts a diffusely distended biliary tree with no visible mass. Diffuse disease with visible papillary tumor (**d**) Thick-slab MRC image demonstrates a markedly distended central biliary tree with a nodule in the common hepatic duct (*arrow*). Focal disease in peripheral duct (**e**) Axial T1-weighted image with intravenous contrast shows an aneurysmally distended peripheral duct with an enhancing papillary tumor (*arrow*). (**f**) Thick-slab MRC image demonstrates communication of the cystic mass with the biliary tree (*arrow*), differentiating the tumor from biliary cystadenoma

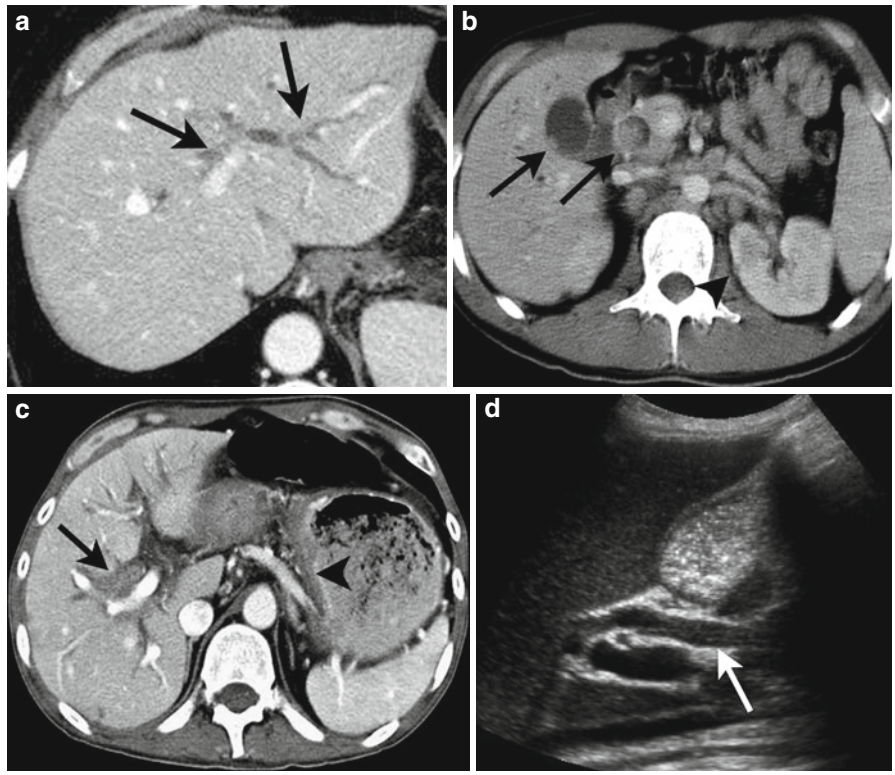

Fig. 81.15 Metastases to the bile ducts. Colon carcinoma (**a**) enhanced CT shows multifocal intraductal tumor (*arrows*) with attenuation higher than bile. Melanoma (**b**) enhanced CT depicts papillary metastases to the CBD and gallbladder (*arrows*). Note the adenopathy and tiny renal cortical metastasis as well (*arrowhead*). Gastric carcinoma (**c**) enhanced CT demonstrates diffuse thickening of the stomach wall (*arrowhead*) and infiltrative periductal tumor diffusely affecting the central biliary tree (*arrow*). Acute lymphoblastic leukemia (**d**) longitudinal ultrasound image of the CBD shows diffuse tumor infiltration of the submucosa narrowing the lumen

identification and assessment of intraductal tumors. Typically, dilated duct or segmental ductal system is followed centrally to the obstructive mass. However, the differentiation of intraductal debris/stones from small papillary tumors may require CEUS. Mucin hypersecreting tumors manifests as focal or diffuse biliary dilatation associated with small papillary tumors that may not be easily seen because of their small size. While CT and MRI cannot distinguish mucin from bile, layering of low-level echoes, sometimes noted on ultrasound, is suggestive of mucin (Fig. 81.14).

CT and MR Scan

MRI holds several advantages to CT in the imaging of intraductal tumors. Contrast-enhanced thin-section MRI is superior to CT to detect enhancement of the small papillary intraductal lesions. MRC is useful to provide comprehensive imaging of diffuse or focal ductal dilatation with papillary projections in intraductal-growing CC with mucin hypersecretion (Fig. 81.14). MRC is also helpful to demonstrate a communication between a bile duct and cystic dilatation of a mucin-filled intrahepatic bile duct, which allows its differentiation from biliary cystadenoma.

Other Causes of Malignant Biliary Obstruction

Aside from CC, malignant biliary obstruction can result from metastases to the biliary tree or compression/invasion of bile ducts by tumors in adjacent organs.

Metastases to the biliary tree mimic the appearances of CC and thus can appear as intraductal papillary tumors or periductal infiltrative disease. The most common intraductal papillary metastases are colon carcinoma (often with synchronous or prior hepatic metastases) and melanoma (Fig. 81.15). Periductal infiltrative metastases include gastric (often signet-ring cell type), breast (especially lobular carcinoma), lung, and advanced lymphoma/leukemia. The imaging pattern caused by intraductal metastasis may not be distinguishable from primary CC on cross-sectional

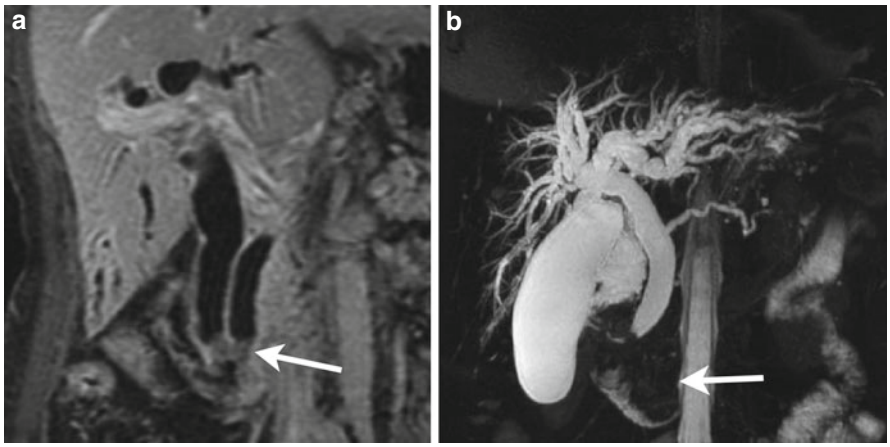

Fig. 81.16 Ampullary carcinoma. (**a**) Coronal enhanced T1-weighted MRI shows a small enhancing mass (*arrow*) causing obstruction of the distal CBD and pancreatic ducts. (**b**) MIP image of T2-weighted respiratory-triggered three-dimensional MRC depicts a large polypoid mass (*arrow*) protruding into the duodenal lumen

imaging (Fig. 81.15) (Moon et al. 2003). The presence of metastases elsewhere and knowledge of past history of primary malignancy are clues to the correct diagnosis.

Invasion of the intrahepatic bile ducts is occasionally seen in primary hepatic malignancies, especially hepatocellular carcinoma. At the hepatic hilum or mid-CBD level (within the hepatoduodenal ligament), nodal metastases, commonly from the stomach, pancreas, colon, lung, lymphoma, and breast, may obstruct the duct. Periductal nodal masses are seen on imaging in the majority of the cases. Within the pancreas, the CBD is commonly obstructed by primary pancreatic neoplasms, especially adenocarcinoma.

At the level of the ampulla, malignant obstruction can be caused by four primary tumors: pancreatic adenocarcinoma, CC, duodenal carcinoma, and ampullary carcinoma. The first three are discussed elsewhere. Ampullary carcinoma is usually small when diagnosed because it causes obstructive symptoms at an early stage. However, identification of small ampullary tumors with imaging is a challenge. Contrast-enhanced coronal CT or MR imaging is helpful to identify an ampullary mass (Fig. 81.16); however, it is often difficult to differentiate between an ampullary tumor and a prominent or edematous ampulla. Irregular and asymmetric narrowing of the distal common bile duct and diffuse marked biliary dilatation on MRC or coronal CT images are findings suggestive of ampullary carcinoma (Chung et al. 2011). Endoscopic retrograde cholangiopancreatography (ERCP) with endoscopic biopsy is the method of choice for confirming ampullary carcinoma.

Conclusion

There have been great advances in the understanding of the various morphologic types of CC and in the imaging techniques used for diagnosis and staging. Ultrasound is reliable in detecting biliary dilatation and malignant obstruction which prompts further imaging with CT or MRI. Contrast-enhanced ultrasound may be used as a problem-solving method in difficult cases such as intraductal-growing CC with mucin hypersecretion. Thin-section, contrast-enhanced MSCT facilitated by MPR images has been established as the main imaging modality for staging CC and malignant biliary obstruction. MRC provides a comprehensive overview of biliary obstruction and reliable information about the tumor extent in the bile duct. The combined use of MRC and thin-section contrast-enhanced MR imaging is a useful alternative to MSCT for staging CC and malignant biliary obstruction.

References

Asayama Y, Yoshimitsu K, Irie H, et al. Delayed-phase dynamic CT enhancement as a prognostic factor for mass-forming intrahepatic cholangiocarcinoma. Radiology. 2006;238:150–5.

Bhayana D, Kim TK, Jang HJ, Burns PN, Wilson SR. Hypervascular liver masses on contrast-enhanced ultrasound: the importance of washout. AJR Am J Roentgenol. 2010;194:977–83.

Burak K, Angulo P, Pasha TM, Egan K, Petz J, Lindor KD. Incidence and risk factors for cholangiocarcinoma in primary sclerosing cholangitis. Am J Gastroenterol. 2004;99:523–6.

Chen HW, Pan AZ, Zhen ZJ, et al. Preoperative evaluation of resectability of Klatskin tumor with 16-MDCT angiography and cholangiography. AJR Am J Roentgenol. 2006; 186:1580–6.

Cho ES, Park MS, Yu JS, Kim MJ, Kim KW. Biliary ductal involvement of hilar cholangiocarcinoma: multidetector computed tomography versus magnetic resonance cholangiography. J Comput Assist Tomogr. 2007;31:72–8.

Choi BI, Kim TK, Han JK. MRI of clonorchiasis and cholangiocarcinoma. J Magn Reson Imaging. 1998;8:359–66.

Choi D, Lim JH, Lee KT, et al. Cholangiocarcinoma and Clonorchis sinensis infection: a case-control study in Korea. J Hepatol. 2006;44:1066–73.

Chung YE, Kim MJ, Kim HM, et al. Differentiation of benign and malignant ampullary obstructions on MR imaging. Eur J Radiol. 2011;80:198–203.

Han JK, Choi BI, Kim AY, et al. Cholangiocarcinoma: pictorial essay of CT and cholangiographic findings. Radiographics. 2002;22:173–87.

Khalili K, Metser U, Wilson SR. Hilar biliary obstruction: preliminary results with Levovist-enhanced sonography. AJR Am J Roentgenol. 2003;180:687–93.

Kim TK, Choi BI, Han JK, Jang HJ, Cho SG, Han MC. Peripheral cholangiocarcinoma of the liver: two-phase spiral CT findings. Radiology. 1997;204:539–43.

Kim JH, Kim TK, Eun HW, et al. CT findings of cholangiocarcinoma associated with recurrent pyogenic cholangitis. AJR Am J Roentgenol. 2006;187:1571–7.

Kim SJ, Lee JM, Han JK, Kim KH, Lee JY, Choi BI. Peripheral mass-forming cholangiocarcinoma in cirrhotic liver. AJR Am J Roentgenol. 2007;189:1428–34.

Kim H, Lim JH, Jang KT, et al. Morphology of intraductal papillary neoplasm of the bile ducts: radiologic-pathologic correlation. Abdom Imaging. 2011;36:438–46.

Lee SS, Kim MH, Lee SK, et al. MR cholangiography versus cholangioscopy for evaluation of longitudinal extension of hilar cholangiocarcinoma. Gastrointest Endosc. 2002;56:25–32.

Lee HY, Kim SH, Lee JM, et al. Preoperative assessment of resectability of hepatic hilar cholangiocarcinoma: combined CT and cholangiography with revised criteria. Radiology. 2006;239:113–21.

Lim JH. Cholangiocarcinoma: morphologic classification according to growth pattern and imaging findings. AJR Am J Roentgenol. 2003;181:819–27.

Malhi H, Gores GJ. Cholangiocarcinoma: modern advances in understanding a deadly old disease. J Hepatol. 2006; 45:856–67.

Masselli G, Manfredi R, Vecchioli A, Gualdi G. MR imaging and MR cholangiopancreatography in the preoperative evaluation of hilar cholangiocarcinoma: correlation with surgical and pathologic findings. Eur Radiol. 2008;18:2213–21.

Moon SG, Han JK, Kim TK, Kim AY, Kim TJ, Choi BI. Biliary obstruction in metastatic disease: thin-section helical CT findings. Abdom Imaging. 2003;28:45–52.

Ohtsuka M, Kimura F, Shimizu H, et al. Similarities and differences between intraductal papillary tumors of the bile duct with and without macroscopically visible mucin secretion. Am J Surg Pathol. 2011;35:512–21.

Park MS, Kim TK, Kim KW, et al. Differentiation of extrahepatic bile duct cholangiocarcinoma from benign stricture: findings at MRCP versus ERCP. Radiology. 2004;233:234–40.

Seo H, Lee JM, Kim IH, et al. Evaluation of the gross type and longitudinal extent of extrahepatic cholangiocarcinomas on contrast-enhanced multidetector row computed tomography. J Comput Assist Tomogr. 2009;33:376–82.

Uchida M, Ishibashi M, Tomita N, Shinagawa M, Hayabuchi N, Okuda K. Hilar and suprapancreatic cholangiocarcinoma: value of 3D angiography and multiphase fusion images using MDCT. AJR Am J Roentgenol. 2005;184:1572–7.

Vilgrain V. Staging cholangiocarcinoma by imaging studies. HPB (Oxf). 2008;10:106–9.

Wilson SR, Kim TK, Jang HJ, Burns PN. Enhancement patterns of focal liver masses: discordance between contrast-enhanced sonography and contrast-enhanced CT and MRI. AJR Am J Roentgenol. 2007;189:W7–12.

Yamasaki S. Intrahepatic cholangiocarcinoma: macroscopic type and stage classification. J Hepatobiliary Pancreat Surg. 2003;10:288–91.